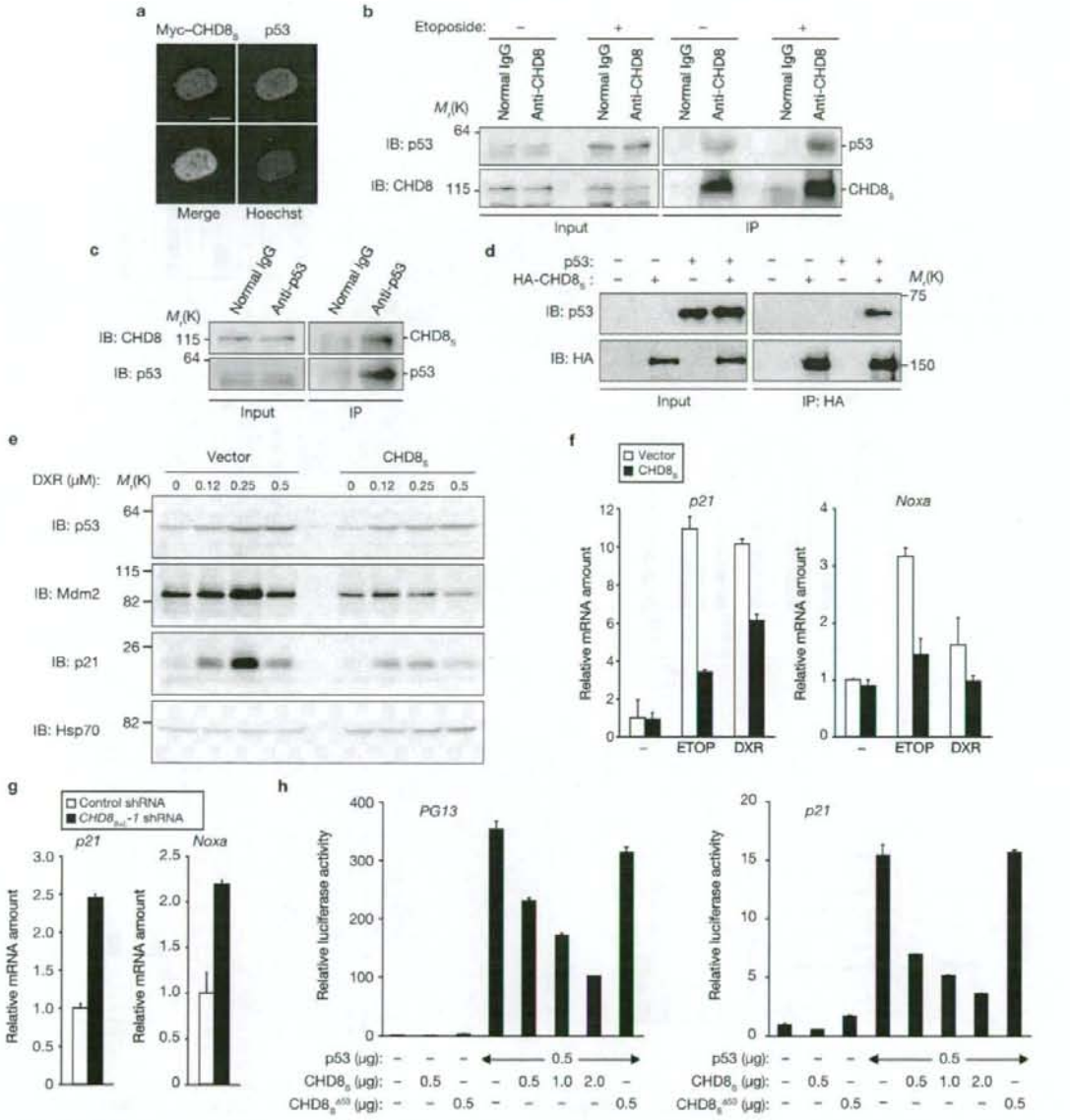

Figure 2 CHD8 interacts with and inhibits transactivation by p53. (**a**) HeLa cells expressing Myc–$CHD8_S$ were immunostained with anti-Myc or p53. Scale bar, 5 μm. (**b**) U2OS cells were incubated with etoposide and then subjected to immunoprecipitation (IP) with an anti-CHD8 antibody, and immunoblot analysis with an anti-p53 antibody. (**c**) Immunoprecipitation of U2OS lysates with anti-p53 and immunoblot analysis with an anti-CHD8 antibodies. (**d**) *In vitro* binding assay for recombinant $CHD8_S$ and p53. (**e**) U2OS cells overexpressing $CHD8_S$ were incubated with doxorubicin (DXR) and then subjected to immunoblot analysis with the indicated antibodies. (**f**) U2OS cells overexpressing $CHD8_S$ were treated with the genotoxic agents DXR (0.5 μM) and etoposide (ETOP, 20 μM) and then subjected to qRT–PCR. (**g**) U2OS cells infected with a retroviral vector encoding *$CHD8_{ex1}$-1* shRNA were subjected to qRT–PCR. (**h**) Luciferase assay using either wild-type or mutant $CHD8_S^{\Delta 53}$. Data are mean ± s.d., $n = 3$ (**f**–**h**).

Given that lack of both $CHD8_S$ and $CHD8_L$ results in widespread apoptosis in mouse embryos[22], we hypothesized that CHD8 may possess anti-apoptotic activity. Indeed, overexpression of either $CHD8_S$ or $CHD8_L$ inhibited the induction of apoptosis in mouse NIH 3T3 cells exposed to etoposide or ultraviolet (UV) radiation (Fig. 1a–c; Supplementary Information, Fig. S2a). The apoptosis-related cleavage of both caspase-3 and poly(ADP-ribose) polymerase (PARP) was also inhibited by overexpression of CHD8

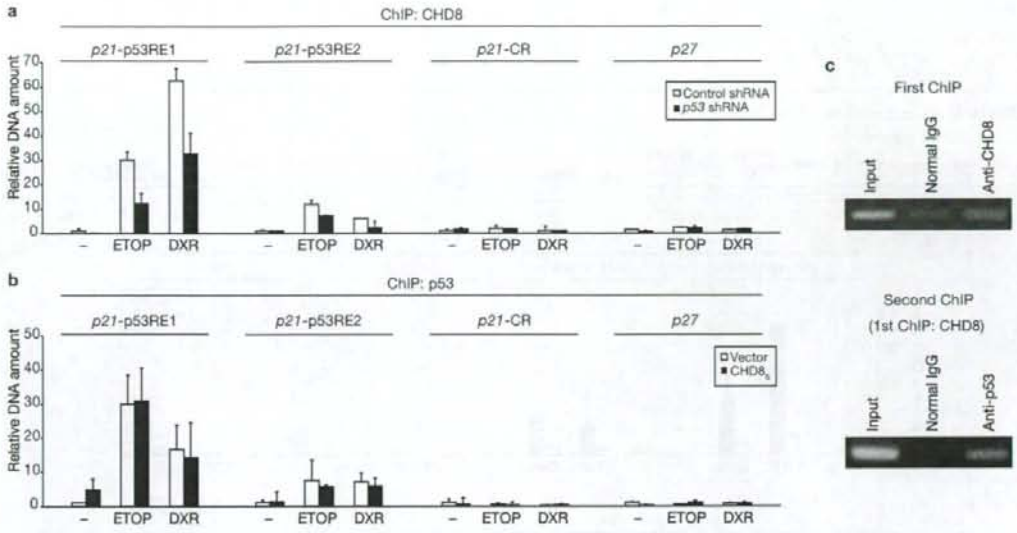

Figure 3 CHD8 binds to the promoters of p53 target genes. (**a**) U2OS cells infected with a retroviral vector encoding *p53* shRNA were incubated with the genotoxic agents etoposide (ETOP, 20 μM) and doxorubicin (DXR, 0.5 μM). The cells were then subjected to ChIP with an anti-CHD8 antibody and the precipitated DNA was quantified by real-time PCR with primers specific for p53-responsive elements (p53REs) 1 or 2 or a control region (CR) of the *p21* promoter or for the *p27* promoter. (**b**) U2OS cells overexpressing $CHD8_S$ were treated with ETOP (20 μM) and DXR (0.5 μM) and subjected to ChIP with an anti-p53 antibody. Data are mean ± s.d., $n = 3$ (**a**, **b**). (**c**) U2OS cells overexpressing $CHD8_S$ were incubated with ETOP and then subjected to ChIP with an anti-CHD8 antibody. The immunoprecipitates were subjected to ChIP with an anti-p53 antibody.

(Supplementary Information, Fig. S2b). CHD8 markedly suppressed apoptosis induced by etoposide, UV radiation or c-Myc, all of which are dependent on p53, but did not affect apoptosis induced by cycloheximide or staurosporine, which are independent of p53 (Fig. 1d). Furthermore, apoptosis induced by overexpression of p53 was inhibited by $CHD8_S$ (Fig. 1e) or $CHD8_L$ (Supplementary Information, Fig. S3a).

Conversely, depletion of both $CHD8_S$ and $CHD8_L$ by RNA interference (RNAi) induced cell death in U2OS human osteosarcoma cells (Fig. 1f), which harbour wild-type *p53* alleles, as well as in HeLa and HCT116 cells (Supplementary Information, Fig. S3b–d). Depletion of $CHD8_L$ alone had no such effect. We confirmed that cell death triggered by depletion of CHD8 is due to apoptosis (Supplementary Information, Fig. S2c, d). Together, these observations indicate that both $CHD8_S$ and $CHD8_L$ possess anti-apoptotic activity and that the presence of $CHD8_S$ alone in cells is sufficient to prevent apoptosis, suggesting that the anti-apoptotic activity of CHD8 is dependent on the common region of $CHD8_S$ and $CHD8_L$. Apoptosis induced by depletion of CHD8 was blocked by the caspase inhibitor Z-VAD-fmk and was associated with retardation of cell growth (Supplementary Information, Fig. S2e, f).

To investigate whether the apoptosis induced by CHD8 depletion was dependent on p53, we depleted U2OS cells of both CHD8 and p53 and found that additional depletion of p53 in cells depleted of CHD8 restored cell survival (Fig. 1f). Depletion of CHD8 resulted in a marked increase in apoptosis in $p53^{+/+}$ MEFs, but had virtually no effect in $p53^{-/-}$ MEFs (Fig. 1g, h), indicating that CHD8 depletion results in p53 activation. These data thus indicate that CHD8 is an anti-apoptotic molecule and a negative regulator of p53.

CHD8 interacts with and inhibits p53

The subcellular localization of $CHD8_S$ was found to be almost identical to that of p53, with both proteins being largely restricted to the nucleus (Fig. 2a). Reciprocal co-immunoprecipitation analysis revealed that endogenous CHD8 specifically interacted with endogenous p53 in U2OS cells (Fig. 2b, c; Supplementary Information, Fig. S3e). Similar experiments with a series of deletion mutants of $CHD8_S$ revealed that the N-terminal region of CHD8 is responsible for binding to p53 (Supplementary Information, Fig. S4a). Reciprocal analysis showed that CHD8 binds to the central core domain of p53 (Supplementary Information, Fig. S4b). Furthermore, pulldown assays revealed that recombinant $CHD8_S$ and recombinant p53 bound to each other *in vitro*, suggesting that the interaction is direct (Fig. 2d).

We next examined whether CHD8 affects transcriptional activation by p53 in U2OS cells. Overexpression of $CHD8_S$ or $CHD8_L$ markedly inhibited the etoposide- or doxorubicin-induced upregulation of Mdm2, p21 and Noxa, all of which are encoded by p53 target genes, in U2OS cells (Fig. 2e, f; Supplementary Information, Figs S3f, S5a–c). In contrast, depletion of CHD8 resulted in an increase in the expression of p53 target genes, including those for *p21* and *Noxa* (Fig. 2g), suggesting that CHD8 antagonizes p53 function. Furthermore, overexpression of $CHD8_S$ inhibited in a concentration-dependent manner the p53-induced increase in luciferase activity in human osteosarcoma SaOS2 cells (*p53*-null) harbouring a *luciferase* gene fused to the promoter of the p53 target genes for *p21* or *PG13* (Fig. 2h). $CHD8_S$ overexpression did not affect the activity of a *p21* promoter in which the two p53 binding sites are mutated (Supplementary Information, Fig. S5d). The inhibitory effect of $CHD8_S$ was not mimicked by the $CHD8_S^{\Delta 53}$ mutant (Fig. 2h; Supplementary Information, Fig. S5d), which lacks

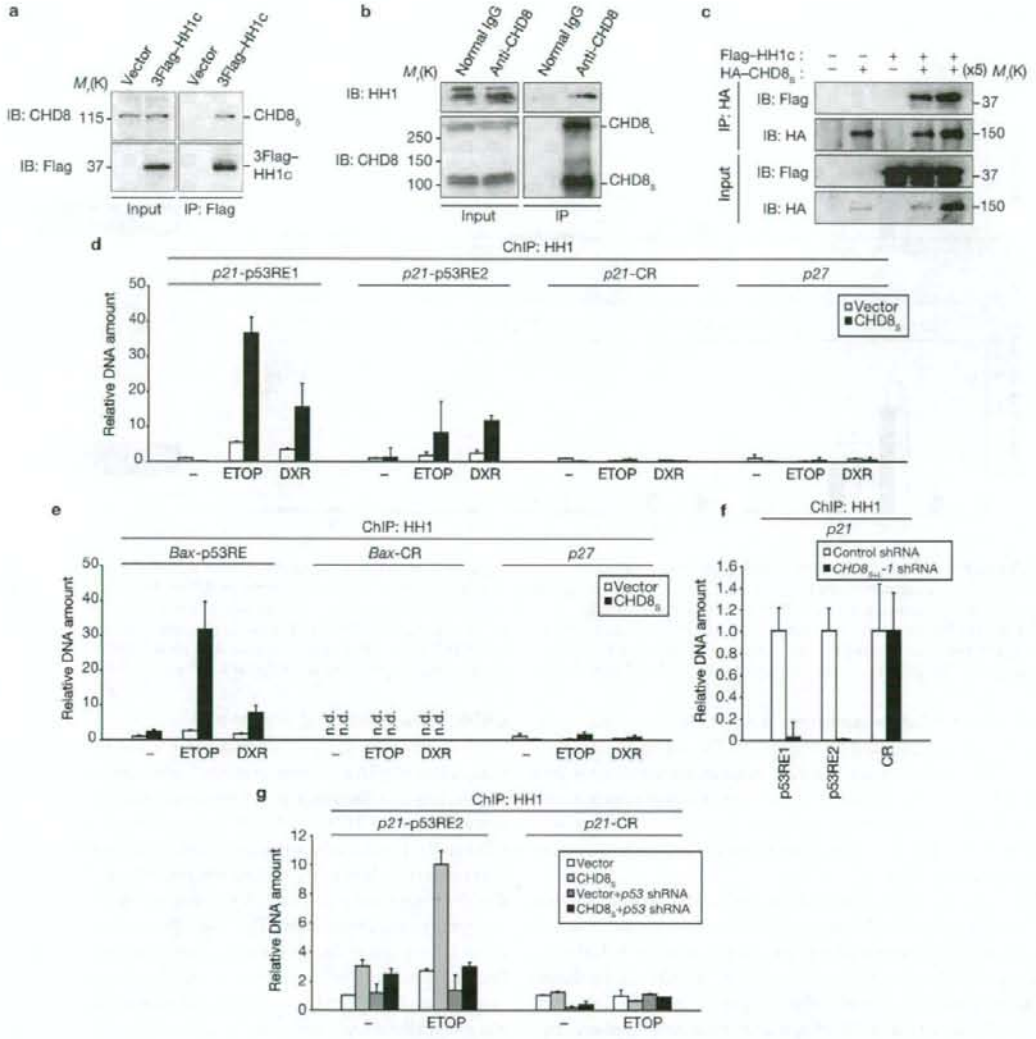

Figure 4 CHD8 recruits histone H1 to the promoters of p53 target genes. (**a**) HEK293T cells expressing 3 × Flag–histone H1c were subjected to immunoprecipitation with anti-Flag and immunoblot analysis with anti-CHD8 antibodies. (**b**) Immunoprecipitation of HEK293T lysates with anti-CHD8 and immunoblot analysis with anti-histone H1 antibodies. (**c**) *In vitro* binding assay for recombinant CHD8$_S$ and histone H1c. (**d**) U2OS cells overexpressing CHD8$_S$ were treated with the genotoxic agents etoposide (ETOP, 20 μM) and doxorubicin (DXR, 0.5 μM) and subjected to ChIP with an anti-histone H1 antibody. (**e**) ChIP was performed for the *BAX* promoter (n.d., not detected). (**f**) U2OS cells infected with a retroviral vector for *CHD8$_{ex1}$-1* shRNA were subjected to ChIP. (**g**) U2OS cells overexpressing CHD8$_S$ were infected with a retroviral vector for *p53* shRNA, incubated with ETOP and then subjected to ChIP. Data are mean ± s.d., $n = 3$ (**d**–**g**).

the p53-binding domain (Supplementary Information, Fig. S5e), suggesting that binding of CHD8 to p53 is required for suppression of p53 function. CHD8$_S$ did not affect the activity of the transcription factor NF-κB induced by TRAF2 (Supplementary Information, Fig. S5f), suggesting that it is not a general inhibitor of transcription but rather, a specific inhibitor of p53-dependent transactivation. Together, these data indicate that CHD8 interacts with p53 and thereby negatively regulates its function.

CHD8 recruits histone H1 to inhibit p53

We next investigated the possible association of CHD8 and p53 with the promoter regions of p53 target genes using chromatin immunoprecipitation (ChIP; Supplementary Information, Fig. S6). ChIP using anti-CHD8 antibodies revealed that CHD8 specifically associated with p53-responsive elements 1 and 2 of the *p21* promoter in U2OS cells treated with etoposide or doxorubicin but not in untreated cells (Fig. 3a). No substantial association of CHD8 with a control region of the *p21*

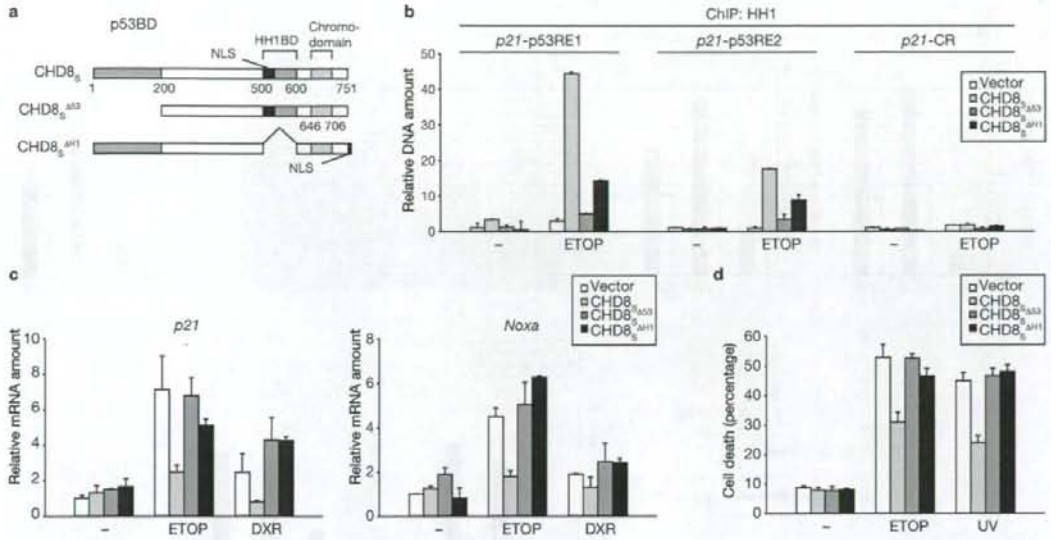

Figure 5 Interaction of CHD8 with p53 and histone H1 is necessary for recruitment of histone H1 to the promoters of p53 target genes. (**a**) Schematic representation of $CHD8_S$ derivatives. (**b**–**d**) U2OS cells overexpressing $CHD8_S$ derivatives were exposed to genotoxic stress (etoposide, ETOP, 20 μM and doxorubicin, DXR, 0.5 μM) and then subjected to ChIP (**b**), qRT–PCR (**c**) and trypan blue staining (**d**). Data are mean ± s.d., $n = 3$.

promoter that does not bind p53 or with the *p27* promoter was detected. Moreover, depletion of *p53* by RNAi reduced the extent of CHD8 association with the p53-responsive elements of the *p21* promoter, suggesting that p53 mediates the association of CHD8 with chromatin. ChIP using anti-p53 antibodies revealed that $CHD8_S$ overexpression did not affect the association of p53 with chromatin in response to genotoxic stress (Fig. 3b), suggesting that p53 binds to the *p21* promoter in a CHD8-independent manner. A sequential ChIP experiment revealed that p53 and CHD8 occupy the *p21* promoter region simultaneously (Fig. 3c).

To elucidate the mechanism by which CHD8 inhibits p53 function, we attempted to identify molecules that associate with Flag–$CHD8_S$ in HEK293T cells using a 'shotgun' proteomics approach. The results of several independent experiments revealed that histone H1 was consistently the most prominent of the proteins associated with immunoprecipitated Flag–$CHD8_S$ (Supplementary Information, Table S1). Reciprocal co-immunoprecipitation analysis showed that Flag-tagged histone H1c interacted with endogenous CHD8 (Fig. 4a). We also confirmed that endogenous CHD8 associated with endogenous histone H1 (Fig. 4b). Furthermore, pulldown assays revealed that recombinant $CHD8_S$ and recombinant histone H1c bound to each other *in vitro*, suggesting that the interaction is direct (Fig. 4c). We examined which histone H1 subtypes interact with CHD8 in a co-immunoprecipitation assay. This analysis revealed that all five major H1 subtypes (H1a, H1b, H1c, H1d, H1e) interacted with $CHD8_S$ (Supplementary Information, Fig. S4c). *In vitro* binding assays with a series of deletion mutants showed that residues 500–600 is the region of $CHD8_S$ required for binding to histone H1 (Supplementary Information, Fig. S4d). The histone H1-binding domain thus includes the nuclear localization signal of $CHD8_S$ and is distinct from the chromodomain at the C terminus.

Given that CHD8 was found to interact with histone H1, we also examined whether histone H1 is recruited to the p53-responsive elements of the *p21* promoter. ChIP using an anti-histone H1 antibody showed that histone H1 was indeed recruited to the *p21* promoter on treatment of U2OS cells with etoposide or doxorubicin, and this effect was markedly enhanced by overexpression of $CHD8_S$ (Fig. 4d). Similar results were obtained with the promoter of the p53 target gene *BAX* (Fig. 4e). Conversely, depletion of either CHD8 or p53 markedly reduced the amount of histone H1 associated with the *p21* promoter (Fig. 4f, g). This series of ChIP experiments thus suggests that a p53–CHD8–histone H1 complex forms at the promoters of p53-inducible genes in response to genotoxic stress.

p53–CHD8–histone H1 complex is necessary for suppression of p53 function

We next examined the ability of CHD8 mutants that lack either the p53 binding domain ($CHD8_S^{\Delta 53}$) or the histone H1 binding domain ($CHD8_S^{\Delta H1}$) to recruit histone H1 to the promoters of p53 target genes (Fig. 5a). Given that the $CHD8_S^{\Delta H1}$ mutant lacks residues 500–600, which include the nuclear localization signal, we added the nuclear localization signal of the large T antigen of simian virus 40 to the C terminus of the mutant protein. Deletion of either of the two binding domains markedly impaired the ability of $CHD8_S$ to recruit histone H1 to the p53-responsive elements of the *p21* promoter (Fig. 5b). Furthermore, neither $CHD8_S^{\Delta 53}$ nor $CHD8_S^{\Delta H1}$ had an inhibitory effect on p53-dependent transactivation (Fig. 5c) or apoptosis (Fig. 5d). Together, these data suggest that CHD8 recruits histone H1 to p53-responsive elements, and that such recruitment of histone H1 results in suppression of transcriptional activation by p53.

Histone H1 is essential for repression of p53-dependent transcription

Our observation that the $CHD8_S^{\Delta H1}$ mutant is unable to repress p53 function led us to investigate the requirement for histone H1 in such repression. To this end, we adopted three independent approaches.

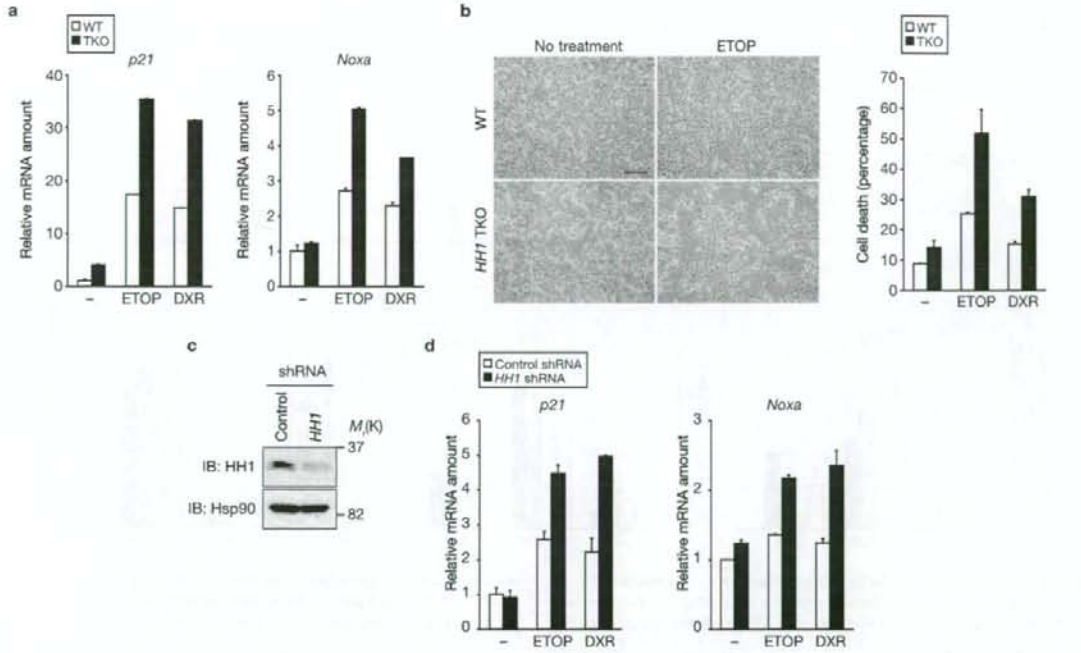

Figure 6 Requirement for histone H1 in repression of p53-mediated transcription. (**a**, **b**) Wild-type (WT) or *HH1c*$^{-/-}$*HH1d*$^{-/-}$*HH1e*$^{-/-}$ triple-knockout (TKO) ES cells were incubated with etoposide (ETOP, μ2 M) and doxorubicin (DXR, 0.05 μM) and then subjected to qRT–PCR (**a**) and trypan blue staining (**b**). (**c**) U2OS cells were infected with a retroviral vector for *histone H1* (*HH1*) shRNA and then subjected to immunoblot analysis. (**d**) The cells were incubated with ETOP (2 μM) and DXR (0.05 μM) and then subjected to qRT–PCR. Data are mean ± s.d., $n = 3$ (**a**, **b**, **d**).

First, CHD8-dependent suppression of p53 function was examined in *HH1c*$^{-/-}$*HH1d*$^{-/-}$*HH1e*$^{-/-}$ triple-knockout (TKO) embryonic stem (ES) cells[23]. Expression of *p21* and *Noxa* genes (Fig. 6a), as well as the level of apoptosis (Fig. 6b) induced by genotoxic stress, were markedly increased in TKO cells, compared with those in control cells. Second, U2OS cells were subjected to RNAi with a short hairpin RNA (shRNA) designed to deplete all five major subtypes of histone H1 (Fig. 6c). Such depletion of histone H1 resulted in a substantial increase in etoposide- or doxorubicin-induced upregulation of *p21* or *Noxa* mRNA levels (Fig. 6d). Third, expression of a dominant-negative mutant of histone H1 (N-fusion) reduced the amount of endogenous histone H1, as described previously[24], and also increased that of p21, resulting in suppression of cell proliferation (Supplementary Information, Fig. S7). Expression of a histone H1 mutant that does not have dominant-negative activity (C-fusion) did not affect the abundance of p21 or cell proliferation. Together, these three lines of evidence support our conclusion that CHD8 negatively regulates p53 function by recruiting histone H1 to the promoters of p53 target genes, resulting in suppression of apoptosis triggered by p53.

Survival of *Chd8*$^{-/-}$*p53*$^{-/-}$ embryos

The abundance of CHD8 mRNA or protein in mouse embryos was greater during early embryogenesis than at later embryonic stages or in newborns (Fig. 7a, b). In addition to mouse embryos, all human and mouse cancer cell lines tested in this study were found to express CHD8 at relatively high levels (Supplementary Information, Fig. S1c, e, f). Given that CHD8 is a negative regulator of p53, we reasoned that the early embryonic death of *Chd8*$^{-/-}$ mice may be attributable to unscheduled activation of p53. To test this hypothesis, we examined whether deletion of *p53* ameliorated the abnormalities of *Chd8*$^{-/-}$ embryos. Most of the *Chd8*$^{-/-}$ mice died *in utero* between E5.5 and E7.5 and none survived beyond E8.5, whereas *Chd8*$^{-/-}$*p53*$^{-/-}$ embryos survived until E10.5 (Supplementary Information, Table S2). Histopathological examination revealed that the growth retardation seen in *Chd8*$^{-/-}$ embryos was markedly less pronounced in *Chd8*$^{-/-}$*p53*$^{-/-}$ and *Chd8*$^{-/-}$*p53*$^{+/-}$ embryos at E7.5 and E8.5 (Fig. 7c). Cells with condensed nuclei were not seen in *Chd8*$^{-/-}$*p53*$^{-/-}$ embryos at E8.5. The extent of recovery was greater in *Chd8*$^{-/-}$*p53*$^{-/-}$ embryos than in *Chd8*$^{-/-}$*p53*$^{+/-}$ embryos, suggesting that it was related to the reduction in the amount of *p53*. Mesoderm formation, a crucial event in early embryonic development that does not occur in *Chd8*$^{-/-}$ mice, was observed in *Chd8*$^{-/-}$*p53*$^{-/-}$ mice (Fig. 7d). *Chd8*$^{-/-}$*p53*$^{-/-}$ embryos died *in utero* at E10.5 and had severe haemorrhage, indicative of a defect in the cardiovascular system (M.N and K.I.N., unpublished data), suggesting that CHD8 also has another function (or functions) that is required for mid-stage embryonic development. We also observed growth of E3.5 embryos (blastocysts) in culture. *Chd8*$^{-/-}$ blastocysts degenerated between E5.5 and E7.5, whereas *Chd8*$^{-/-}$*p53*$^{-/-}$ blastocysts, like wild-type controls, were alive at E9.5 (Fig. 7e). It is thus likely that the embryonic death of *Chd8*$^{-/-}$ mice is attributable to the unscheduled activation of p53-dependent apoptosis.

To investigate the physiological role of CHD8 during early embryogenesis, we examined embryos at various stages. In ES cells (equivalent to E3.5 embryos), endogenous CHD8 was shown to interact with both endogenous p53 (Fig. 8a) and endogenous histone H1 (Fig. 8b). Furthermore,

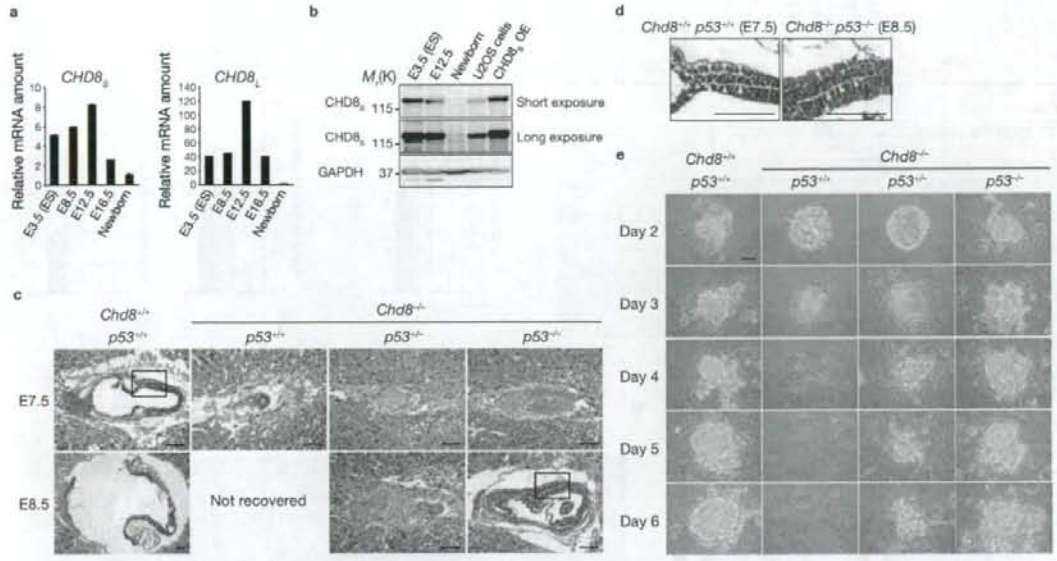

Figure 7 Deletion of *p53* rescues the phenotype of CHD8-deficient mice. (**a**) qRT–PCR for $CHD8_S$ and $CHD8_L$ mRNAs in mouse embryos at the indicated stages. Data are mean ± s.d., $n = 3$. (**b**) Immunoblot analysis of $CHD8_S$ in mouse embryos as well as in U2OS cells and those overexpressing (OE) $CHD8_S$. (**c**) Histopathological examination of $Chd8^{+/+}p53^{+/+}$, $Chd8^{-/-}p53^{+/+}$, $Chd8^{-/-}p53^{+/-}$ and $Chd8^{-/-}p53^{-/-}$ embryos stained with haematoxylin and eosin. (**d**) Higher-magnification views of the boxed regions in **c**. Arrowheads indicate a layer of mesoderm. (**e**) *In vitro* culture of blastocysts of the indicated genotypes. Scale bars are 100 μm (**c**–**e**).

RNAi-mediated depletion of *CHD8* promoted both apoptosis (Fig. 8c, d) and expression of the p53 target genes *p21* and *Noxa* (Fig. 8e). Cultured $Chd8^{-/-}$ blastocysts (equivalent to E5.5 embryos) also showed higher levels of *p21* and *Noxa* mRNAs than did wild-type blastocysts (Fig. 8f). In E7.5 embryos, TUNEL assay showed substantial apoptosis in $Chd8^{-/-}$ embryos, whereas no apoptosis was observed in wild-type or $Chd8^{-/-}p53^{-/-}$ embryos (Fig. 8g). Furthermore, Mdm2 expression was upregulated in $Chd8^{-/-}$ embryos in a p53-dependent manner (Fig. 8h). This genetic evidence supports the notion that CHD8 is a physiological antagonist of p53 *in vivo*, and that loss of CHD8 allows unrestrained p53 activity, which induces apoptosis at the early stage of embryonic development. We therefore propose that the biological role of CHD8 is to suppress unwanted apoptosis during early embryogenesis (Fig. 8i).

DISCUSSION

We have shown that CHD8 negatively regulates p53 function by recruiting histone H1 to the promoters of p53 target genes. Formation of the p53–CHD8–histone H1 complex requires expression of CHD8 and stabilization of p53 by genotoxic stress. CHD8 is preferentially expressed in embryonic tissues and in cancer cell lines that are thought to reflect the embryonic state. Loss of CHD8 induced hyperactivation of p53, resulting in apoptosis, which was prevented by depletion of p53. The biochemical and genetic evidence provided by our study may explain how p53 function is regulated by histone H1.

Histone modification is a fundamental mechanism for epigenetic control of gene expression. The role of core histones in gene regulation has been studied extensively, but that of the linker histone H1 has remained unclear. *In vitro* studies suggest that linker histone molecules influence chromatin structure, nucleosome mobility and gene regulation[25–32]. Histone H1 is not essential for growth or cell division in several unicellular eukaryotes[33–36], but ablation of three of eight genes that encode isoforms of histone H1 in mouse ES cells, resulting in a 50% reduction in histone H1 content, led to embryonic death of the mutant mice[23,37]. Such downregulation of histone H1 elicited marked changes in chromatin structure, including a global reduction in nucleosome spacing, local reduction in chromatin compaction and changes in the modification of core histones. Despite these changes, microarray analysis of the mutant ES cells revealed that expression of only a few genes was altered[23]. These observations suggest that histone H1 participates in the regulation of specific genes that are essential for survival.

In response to genotoxic stress, mammalian cells activate a complex network of proteins, a key element of which is p53. Post-translational modification of p53 results in transcriptional activation of its target genes[1,6,7]. Regulation of p53 by checkpoint signalling was originally thought to be mediated almost exclusively at the post-translational level[1,6,8]. More recently, p53 has also been found to be regulated at the transcriptional[38] and translational[39] levels. We have now uncovered another mode of p53 regulation mediated by CHD8-dependent recruitment of histone H1 to the promoters of its target genes.

Cells proliferate extensively with short G_1 and G_2 phases during early embryogenesis. The DNA replication checkpoint may therefore be readily activated at this time, with the consequent risk of inducing p53-dependent apoptosis. We propose that the biological role of CHD8 is to suppress unwanted apoptosis during early embryogenesis (Fig. 8i). Consistent with this notion, we found that the amounts of CHD8 mRNA and protein are higher during the early and mid phases of mouse embryonic development

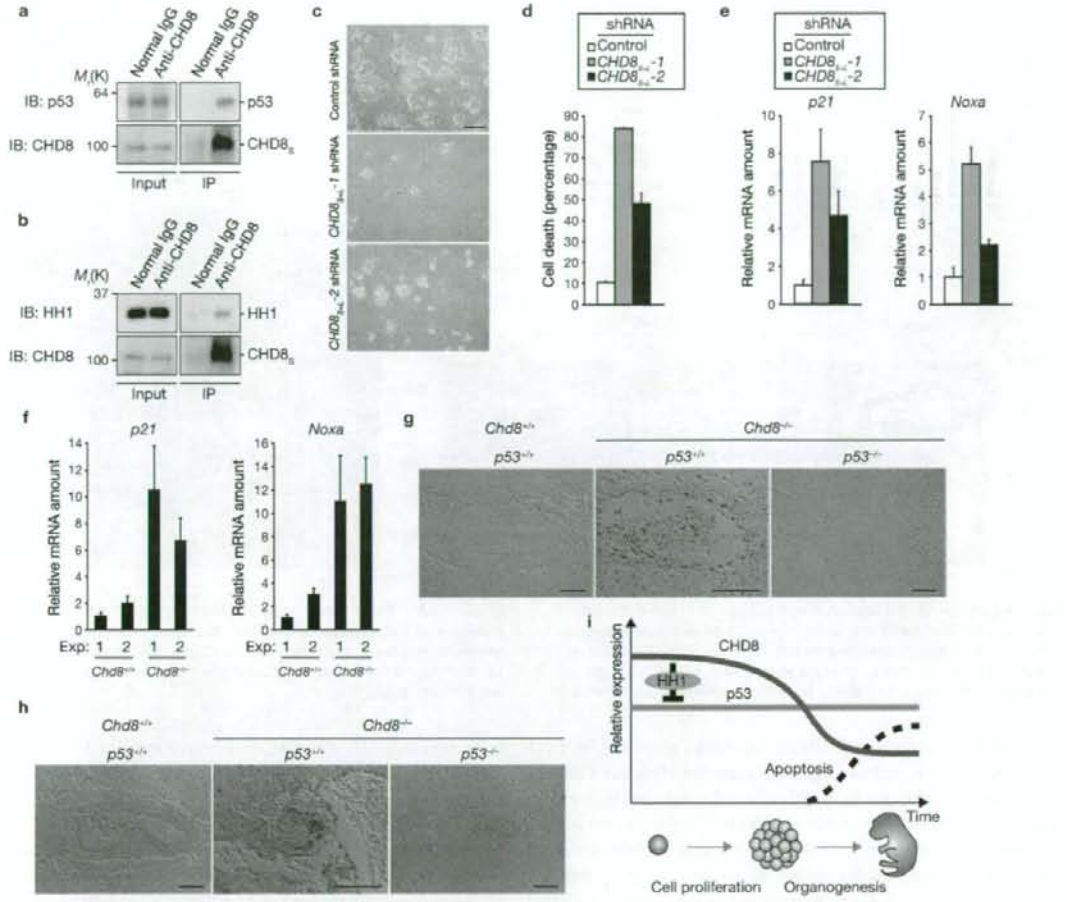

Figure 8 CHD8 sets a threshold for induction of apoptosis during early embryogenesis by counteracting p53 function. (**a**, **b**) Immunoprecipitation of ES cell lysates with an anti-CHD8 antibody, and immunoblot analysis with either anti-p53 (**a**) or anti-histone H1 (**b**) antibodies. (**c**–**e**) ES cells infected with retroviral vectors for *CHD8*$_{shL}$*-1* or *CHD8*$_{shL}$*-2* shRNAs were subjected to trypan blue staining (**c**, quantification shown in **d**) and qRT–PCR (**e**). (**f**) *Chd8*$^{+/+}$ or *Chd8*$^{-/-}$ blastocysts were subjected to qRT–PCR for *p21* and *Noxa*. Data are mean ± s.d., $n = 3$ (**d**–**f**). (**g**, **h**) Sections of *Chd8*$^{+/+}$*p53*$^{+/+}$, *Chd8*$^{-/-}$*p53*$^{+/+}$ and *Chd8*$^{-/-}$*p53*$^{-/-}$ embryos were subjected to TUNEL assay (**g**) or to immunohistochemistry (**h**) with anti-Mdm2 antibody. Scale bars are 100 μm (**c**, **g**, **h**). (**i**) Model for the biological role of CHD8. When cells proliferate extensively during early embryogenesis, CHD8 is expressed at high levels and suppresses p53 function through histone H1 recruitment to prevent unwanted apoptosis. Once the level of CHD8 expression decreases, during mid to late embryogenesis, some cells undergo apoptosis for organogenesis.

than in newborns. Genetic ablation of CHD8 results in extensive p53-dependent apoptosis in mouse embryos at a stage when *Chd8* is expressed at high levels in wild-type mice. On the other hand, apoptosis is necessary for organogenesis, which occurs mainly during mid to late embryogenesis, when the level of *Chd8* expression decreases. CHD8 may therefore regulate a threshold for apoptosis induction in a developmental-stage-specific manner: The threshold for apoptosis triggered by p53 is high during early embryogenesis, whereas it is lower after the mid-stage. In cancer cell lines, the level of CHD8 is relatively high, suggesting that cancer cells generally show an undifferentiated phenotype and reflect embryonic stages of development, or that cells expressing CHD8 may have a selective advantage in terms of cell growth or acquisition of immortality as a result of the suppressing p53 function. Thus we suggest that p53 function is, at least in part, suppressed by CHD8 in such cancer cell lines. Furthermore, haploinsufficiency at the *CHD8* locus was recently implicated in the pathogenesis of a human developmental anomaly[40], providing further genetic evidence in support of a crucial role for CHD8 in development.

METHODS

Antibodies. Anti-p53 (FL393, Pab240), anti-Mdm2 (SMP14) and anti-His$_6$ (H15) antibodies were obtained from Santa Cruz Biotechnology; anti-caspase-3 cleaved at Asp-175 and anti-PARP antibodies were from Cell Signalling; anti-histone H1 antibodies were from Abcam; anti-p21 antibodies from BD Pharmingen; anti-Hsp70 and anti-Hsp90 antibodies from Transduction Laboratories; anti-HA (HA11) antibodies from Babco; anti-Myc (9E10) antibodies from Roche; anti-Flag (M2) from Sigma; anti-α-tubulin (TU01) antibodies from Zymed; anti-glyceraldehyde-3-phosphate dehydrogenase (GAPDH; 1D4) from Stressgen; and anti-CHD8 antibodies were generated by A. Kikuchi (Hiroshima University). Alexa 488- or

Alexa 546-conjugated goat antibodies to mouse or rabbit IgG were obtained from Molecular Probes. Antibodies were used at a dilution of 1:2,000.

Plasmids. Complementary DNAs encoding wild-type or mutant forms of mouse $CHD8_S$ or human $CHD8_S$, each tagged at its N terminus with Flag, Myc or HA epitopes, were subcloned into pcDNA3 (Invitrogen). Complementary DNAs encoding wild-type or mutant forms of human p53, each tagged at its N terminus with the HA epitope, were subcloned into pCGN. Complementary DNAs encoding mouse histone H1 variants, each tagged at its N terminus with three copies of the Flag epitope, were subcloned into pcDNA3. His_6-tagged proteins were expressed in *Escherichia coli* strain BL21(DE3)pLys(S) (Novagen).

Cell culture, transfection and infection. HEK293T, HeLa, HCT116, U2OS and SaOS2 cells were cultured in an atmosphere of 5% CO_2 at 37°C in Dulbecco's modified Eagle's medium (DMEM, Invitrogen) supplemented with 10% fetal bovine serum (Invitrogen). NIH 3T3 cells were cultured under the same conditions in DMEM supplemented with 10% bovine serum (Invitrogen). MEFs and ES cells were cultured as described previously[41,42]. HEK293T, HeLa and SaOS2 cells were transfected with vectors using FuGENE6 (Roche). For retroviral infection, cDNAs were subcloned into pMX-puro.

Immunoprecipitation and immunoblot analysis. Cell lysis, immunoprecipitation and immunoblot analysis were performed as described previously[43]. For solubilization of chromatin-bound histone H1, cells were suspended in a solution containing 50 mM Tris-HCl (pH 7.5), 0.5% Triton X-100, 300 mM NaCl, 60 mM $MgCl_2$, 10 mM $CaCl_2$ and DNase I (167 U ml^{-1}, Roche) and then incubated at 30 °C for 50 min.

Induction of apoptosis. Cells were incubated with etoposide (50 μM; Sigma) for 24 h, with cycloheximide (100 μg ml^{-1}; Wako) for 24 h, with staurosporine (1 μM; Sigma) for 5 h or with doxorubicin (0.5 μM or the indicated concentrations; Sigma) for 24 h. Cells were exposed to UV radiation (50 J/m^2) with an ultraviolet crosslinker UVC500 (Hoefer) and examined after 12 h.

RNAi. The retroviral vector for expression of shRNAs was described previously[43]. The hairpin sequences specific for human or mouse *CHD8* ($CHD8_{S+L}$-*1*, $CHD8_{S+L}$-*2*, $CHD8_S$-*1*, $CHD8_S$-*2*), for human *p53*, for human *histone H1A* (also effective for *H1B*, *H1C*, *H1D* and *H1E*, given the high similarity of the target region) and for enhanced green fluorescent protein (*EGFP*, Clontech) mRNAs corresponded to nucleotides 138–158 ($CHD8_{S+L}$-*1*), 814–834 ($CHD8_{S+L}$-*2*), 3808–3828 ($CHD8_L$-*1*), 4413–4433 ($CHD8_L$-*2*), 775–793 (*p53*), 262–282 (*histone H1A*) and 126–146 (*EGFP*) of the respective coding regions. The resulting vectors were used to transfect Plat E cells and thereby to generate recombinant retroviruses.

Protein identification by LC–MS/MS analysis. $CHD8_S$-associated proteins were digested with *Achromobacter* protease I and the resulting peptides were analysed with a nanoscale liquid chromatography–tandem mass spectrometry (LC–MS/MS) system as described previously[44].

Reverse transcription–polymerase chain reaction (RT–PCR) and luciferase assays. RT–PCR analysis and luciferase assays were performed as described previously[45]. Purification of mRNA from cultured blastocysts was performed with a TurboCapture mRNA kit (Qiagen). The primer sequences for RT–PCR are listed in Supplementary Information, Table S3. For luciferase assays, SaOS2 cells were transfected using FuGENE6 with expression vectors encoding human p53 or Flag-tagged wild-type or mutant versions of mouse $CHD8_S$ together with pRLTk (Promega) as an internal control and *luciferase* reporter plasmids containing promoter sequences of *PG13* or human *p21* (wild-type or mutant) genes. The cells were collected 24 h after transfection, lysed and assayed for luciferase activity with a dual-luciferase reporter assay system (Promega).

ChIP. ChIP assays were performed with a ChIP assay kit (Upstate Biotechnology) and 10^6 cells for each reaction. Precipitated DNA was quantified by real-time PCR as described previously[45]. The primer sequences are listed in Supplementary Information, Table S3.

Generation of $Chd8^{+/-}p53^{-/-}$ mice, histopathology and culture of pre-implantation embryos. $Chd8^{+/-}$ mice generated in our laboratory[22] were crossed with $p53^{-/-}$ mice (Taconic Biotechnology). All mice used in this study were backcrossed to the C57BL/6 background for more than six generations. Histopathological analysis, TUNEL assay, immunohistochemistry and culture of pre-implantation embryos were performed as described previously[22]. The primer sequences for genotyping of embryos by nested PCR are listed in Supplementary Information, Table S3. All animal experiments were performed in accordance with institutional guidelines.

Note: Supplementary Information is available on the Nature Cell Biology website.

ACKNOWLEDGEMENTS

We thank T. Kitamura for pMX-puro; J. M. Cunningham and K. Hanada for the mCAT-1 plasmid; S. Miyake for the *PG13-*, *p21-*, and *p21* mutant–Luc plasmids; T. Takemori for the *NF-κB* Luc plasmid; F. Ishikawa and R. Funayama for the N-fusion and C-fusion plasmids; M. Kitagawa for HCT116 and SaOS2 cells; M. Sato, Y. Yamada, T. Moroishi, Y. Katayama, N. Nishimura and K. Oyamada for technical assistance; M. Kimura and A. Ohta for help with preparation of the manuscript; and T. Ushijima, K. Hayashi and members of the authors' laboratories for discussion. K.I.N. was supported by Takeda Science Foundation. Y.F. and A.I.S. were supported by NIH grant CA79057. Y.F. is a GCC Cancer Scholar supported by Georgia Cancer Coalition.

AUTHOR CONTRIBUTIONS

M.N. performed and planned all experiments, except some of ChIP and co-immunoprecipitation experiments, which were performed by K.O., Y.T. and T. Nakagawa; K.I.N. coordinated the study, oversaw the results and wrote the manuscript; S.I. and T. Natsume contributed to proteomic analysis; Y.F. and A.I.S. provided histone H1 triple-knockout cells and many suggestions; A.K. provided antibodies to CHD8. All authors discussed the results and commented on the manuscript.

COMPETING FINANCIAL INTERESTS

The authors declare no competing financial interests.

Published online at http://www.nature.com/naturecellbiology/
Reprints and permissions information is available online at http://npg.nature.com/reprintsandpermissions/

1. Vousden, K. H. & Lu, X. Live or let die: the cell's response to p53. *Nature Rev. Cancer* **2**, 594–604 (2002).
2. Harris, S. L. & Levine, A. J. The p53 pathway: positive and negative feedback loops. *Oncogene* **24**, 2899–2908 (2005).
3. Vogelstein, B., Lane, D. & Levine, A. J. Surfing the p53 network. *Nature* **408**, 307–310 (2000).
4. Laptenko, O. & Prives, C. Transcriptional regulation by p53: one protein, many possibilities. *Cell Death Differ.* **13**, 951–961 (2006).
5. Aylon, Y. & Oren, M. Living with p53, dying of p53. *Cell* **130**, 597–600 (2007).
6. Toledo, F. & Wahl, G. M. Regulating the p53 pathway: *in vitro* hypotheses, *in vivo* veritas. *Nature Rev. Cancer* **6**, 909–923 (2006).
7. Lavin, M. F. & Gueven, N. The complexity of p53 stabilization and activation. *Cell Death Differ.* **13**, 941–950 (2006).
8. Zhang, Y. & Xiong, Y. A p53 amino-terminal nuclear export signal inhibited by DNA damage-induced phosphorylation. *Science* **292**, 1910–1915 (2001).
9. Tanaka, T., Ohkubo, S., Tatsuno, I. & Prives, C. hCAS/CSE1L associates with chromatin and regulates expression of select p53 target genes. *Cell* **130**, 638–650 (2007).
10. Das, S. *et al.* Hzf Determines cell survival upon genotoxic stress by modulating p53 transactivation. *Cell* **130**, 624–637 (2007).
11. Lee, D. *et al.* SWI/SNF complex interacts with tumor suppressor p53 and is necessary for the activation of p53-mediated transcription. *J. Biol. Chem.* **277**, 22330–22337 (2002).
12. Kim, K. *et al.* Isolation and characterization of a novel H1.2 complex that acts as a repressor of p53-mediated transcription. *J. Biol. Chem.* **283**, 9113–9126 (2008).
13. Becker, P. B. Nucleosome remodelers on track. *Nature Struct. Mol. Biol.* **12**, 732–733 (2005).
14. Marfella, C. G. & Imbalzano, A. N. The Chd family of chromatin remodelers. *Mutat. Res.* **618**, 30–40 (2007).
15. Hall, J. A. & Georgel, P. T. CHD proteins: a diverse family with strong ties. *Biochem. Cell Biol.* **85**, 463–476 (2007).
16. Pray-Grant, M. G., Daniel, J. A., Schieltz, D., Yates, J. R., 3rd & Grant, P. A. Chd1 chromodomain links histone H3 methylation with SAGA- and SLIK-dependent acetylation. *Nature* **433**, 434–438 (2005).
17. Zhang, L., Schroeder, S., Fong, N. & Bentley, D. L. Altered nucleosome occupancy and histone H3K4 methylation in response to 'transcriptional stress'. *EMBO J.* **24**, 2379–2390 (2005).
18. Flanagan, J. F. *et al.* Double chromodomains cooperate to recognize the methylated histone H3 tail. *Nature* **438**, 1181–1185 (2005).
19. Lusser, A., Urwin, D. L. & Kadonaga, J. T. Distinct activities of CHD1 and ACF in ATP-dependent chromatin assembly. *Nature Struct. Mol. Biol.* **12**, 160–166 (2005).

20. Sakamoto, I. *et al.* A novel β-catenin-binding protein inhibits β-catenin-dependent Tcf activation and axis formation. *J. Biol. Chem.* **275,** 32871–32878 (2000).
21. Ishihara, K., Oshimura, M. & Nakao, M. CTCF-dependent chromatin insulator is linked to epigenetic remodeling. *Mol. Cell* **23,** 733–742 (2006).
22. Nishiyama, M. *et al.* Early embryonic death in mice lacking the β-catenin-binding protein Duplin. *Mol. Cell. Biol.* **24,** 8386–8394 (2004).
23. Fan, Y. *et al.* Histone H1 depletion in mammals alters global chromatin structure but causes specific changes in gene regulation. *Cell* **123,** 1199–1212 (2005).
24. Funayama, R., Saito, M., Tanobe, H. & Ishikawa, F. Loss of linker histone H1 in cellular senescence. *J. Cell Biol.* **175,** 869–880 (2006).
25. Vignali, M. & Workman, J. L. Location and function of linker histones. *Nature Struct. Biol.* **5,** 1025–1028 (1998).
26. Thomas, J. O. Histone H1: location and role. *Curr. Opin. Cell Biol.* **11,** 312–317 (1999).
27. Lusser, A. & Kadonaga, J. T. Strategies for the reconstitution of chromatin. *Nature Methods* **1,** 19–26 (2004).
28. Thoma, F., Koller, T. & Klug, A. Involvement of histone H1 in the organization of the nucleosome and of the salt-dependent superstructures of chromatin. *J. Cell Biol.* **83,** 403–427 (1979).
29. Bednar, J. *et al.* Nucleosomes, linker DNA, and linker histone form a unique structural motif that directs the higher-order folding and compaction of chromatin. *Proc. Natl Acad. Sci. USA* **95,** 14173–14178 (1998).
30. Pennings, S., Meersseman, G. & Bradbury, E. M. Linker histones H1 and H5 prevent the mobility of positioned nucleosomes. *Proc. Natl Acad. Sci. USA* **91,** 10275–10279 (1994).
31. Shimamura, A., Sapp, M., Rodriguez-Campos, A. & Worcel, A. Histone H1 represses transcription from minichromosomes assembled *in vitro*. *Mol. Cell. Biol.* **9,** 5573–5584 (1989).
32. Layboum, P. J. & Kadonaga, J. T. Role of nucleosomal cores and histone H1 in regulation of transcription by RNA polymerase II. *Science* **254,** 238–245 (1991).
33. Shen, X., Yu, L., Weir, J. W. & Gorovsky, M. A. Linker histones are not essential and affect chromatin condensation *in vivo*. *Cell* **82,** 47–56 (1995).
34. Ushinsky, S. C. *et al.* Histone H1 in *Saccharomyces cerevisiae*. *Yeast* **13,** 151–161 (1997).
35. Patterton, H. G., Landel, C. C., Landsman, D., Peterson, C. L. & Simpson, R. T. The biochemical and phenotypic characterization of Hho1p, the putative linker histone H1 of *Saccharomyces cerevisiae*. *J. Biol. Chem.* **273,** 7268–7276 (1998).
36. Ramon, A., Muro-Pastor, M. I., Scazzocchio, C. & Gonzalez, R. Deletion of the unique gene encoding a typical histone H1 has no apparent phenotype in *Aspergillus nidulans*. *Mol. Microbiol.* **35,** 223–233 (2000).
37. Rupp, R. A. & Becker, P. B. Gene regulation by histone H1: new links to DNA methylation. *Cell* **123,** 1178–1179 (2005).
38. Wang, S. & El-Deiry, W. S. p73 or p53 directly regulates human p53 transcription to maintain cell cycle checkpoints. *Cancer Res.* **66,** 6982–6989 (2006).
39. Takagi, M., Absalon, M. J., McLure, K. G. & Kastan, M. B. Regulation of p53 translation and induction after DNA damage by ribosomal protein L26 and nucleolin. *Cell* **123,** 49–63 (2005).
40. Zahir, F. *et al.* Novel deletions of 14q11.2 associated with developmental delay, cognitive impairment and similar minor anomalies in three children. *J. Med. Genet.* **44,** 556–561 (2007).
41. Nakayama, K. *et al.* Mice lacking $p27^{Kip1}$ display increased body size, multiple organ hyperplasia, retinal dysplasia, and pituitary tumors. *Cell* **85,** 707–720 (1996).
42. Nakayama, K. *et al.* Targeted disruption of *Skp2* results in accumulation of cyclin E and $p27^{Kip1}$, polyploidy and centrosome overduplication. *EMBO J.* **19,** 2069–2081 (2000).
43. Kamura, T. *et al.* VHL-box and SOCS-box domains determine binding specificity for Cul2-Rbx1 and Cul5-Rbx2 modules of ubiquitin ligases. *Genes Dev.* **18,** 3055–3065 (2004).
44. Natsume, T. *et al.* A direct nanoflow liquid chromatography-tandem mass spectrometry system for interaction proteomics. *Anal. Chem.* **74,** 4725–4733 (2002).
45. Yada, M. *et al.* Phosphorylation-dependent degradation of c-Myc is mediated by the F-box protein Fbw7. *EMBO J.* **23,** 2116–2125 (2004).

nature
cell biology

DOI: 10.1038/ncb1831

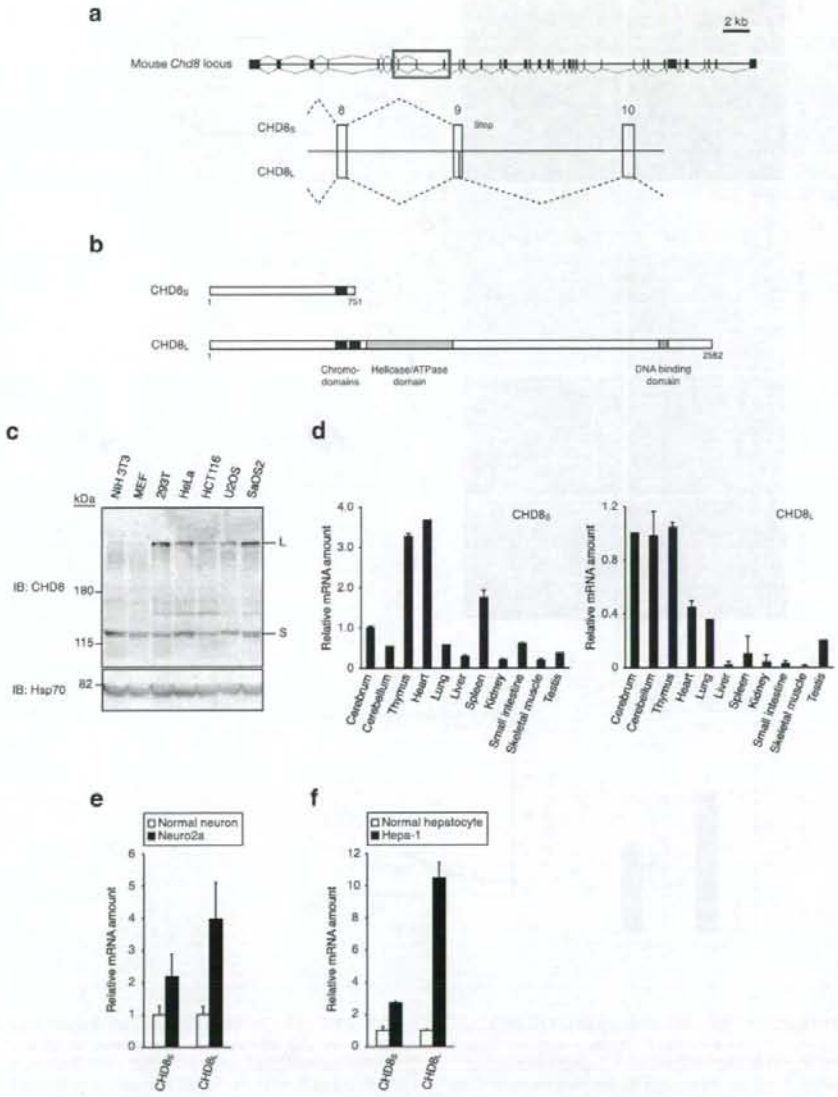

Figure S1 CHD8 has two splicing isoforms. (**a**) Organization of the mouse *Chd8* gene. The region encompassing exons 8 to 10 (red box) and containing the alternative splicing site in exon 9 is expanded in the lower scheme. (**b**) Domain structure of proteins encoded by the two alternative transcripts of *Chd8*. (**c**) Immunoblot analysis of lysates (80 μg of protein) of the indicated cell lines with anti-CHD8 and anti-Hsp70 (loading control). The positions of $CHD8_L$ (L) and $CHD8_S$ (S) are indicated. (**d**) Determination of the amounts of $CHD8_S$ and $CHD8_L$ mRNAs in mouse tissues by quantitative RT-PCR analysis. Data are expressed relative to the corresponding amount of glyceraldehyde-3-phosphate dehydrogenase (GAPDH) mRNA and are means ± SD from three independent experiments. (**e**, **f**) Expression of *Chd8* in mouse cancer cell lines and corresponding normal cells. The amounts of $CHD8_S$ and $CHD8_L$ mRNAs in Neuro2a neuroblastoma cells and normal neurons (**e**) as well as in Hepa-1 hepatoma cells and normal hepatocytes (**f**) were determined by quantitative RT-PCR analysis. Data are means ± SD from three independent experiments.

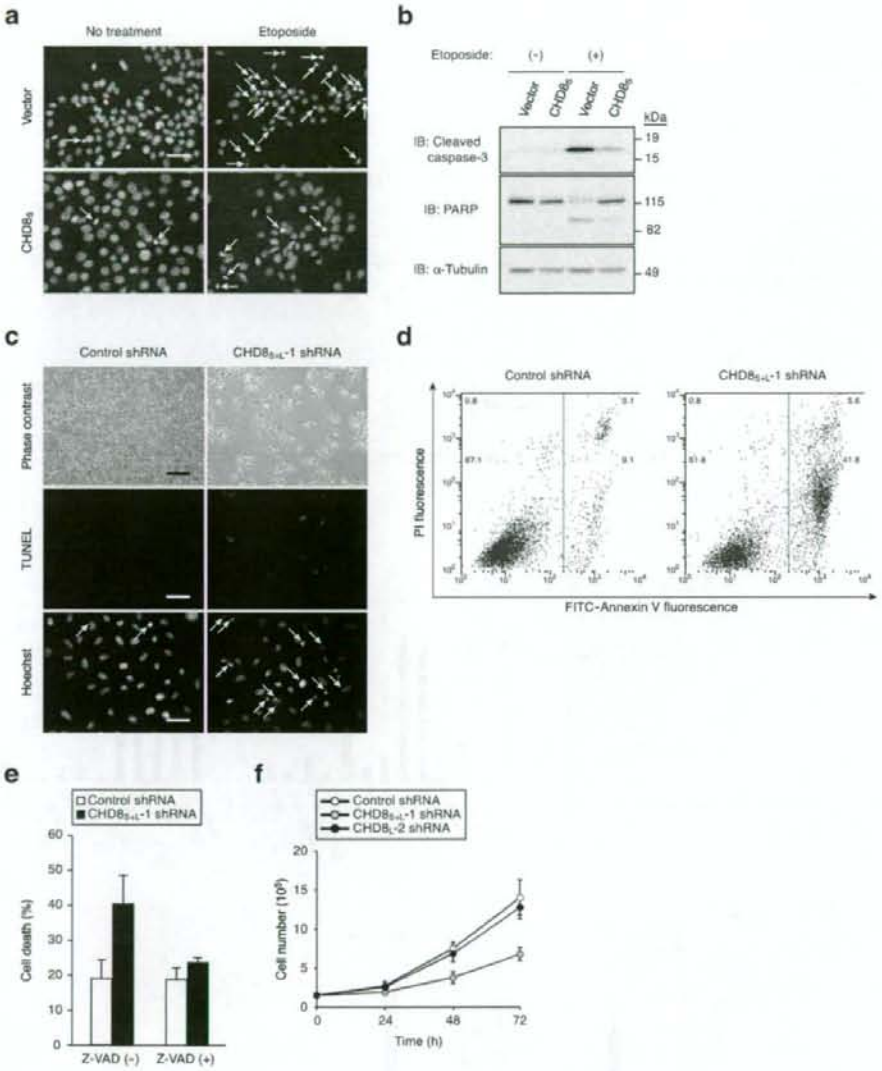

Figure S2 Inhibition of caspase-dependent apoptosis by CHD8. (**a**) NIH 3T3 cells stably infected with a retroviral vector for $CHD8_S$ or with the empty vector were exposed (or not) to etoposide and then stained with Hoechst 33258 for examination of nuclear morphology by fluorescence microscopy. Arrows indicate apoptotic cells with condensed or fragmented nuclei. Scale bar, 20 μm. (**b**) NIH 3T3 cells treated as in (**a**) were lysed and subjected to immunoblot analysis with antibodies to cleaved caspase-3, to PARP, or to α-tubulin (loading control). (**c**) HeLa cells were infected with retroviral vectors for $CHD8_{S+L}$-1 or EGFP (control) shRNAs for 96 h and then either examined by phase-contrast microscopy, subjected to the terminal deoxynucleotidyl transferase–mediated dUTP-biotin nick end-labeling (TUNEL) assay, or stained with Hoechst 33258. Arrows indicate apoptotic cells with condensed or fragmented nuclei. Scale bars, 100 μm (top panels) or 20 μm (middle and bottom panels). (**d**) HeLa cells infected as in (**c**) were stained with fluorescein isothiocyanate (FITC)–labeled Annexin V and propidium iodide (PI) and then analyzed by flow cytometry. (**e**) HeLa cells were infected with retroviral vectors for $CHD8_{S+L}$-1 or EGFP (control) shRNAs for 48 h and then incubated in the absence or presence of 50 μM Z-VAD-fmk (Peptide Institute) for 20 h. The percentage of dead cells was determined by staining with trypan blue. Data are means ± SD from three independent experiments. (**f**) HeLa cells (1.5×10^5) infected with retroviral vectors for $CHD8_{S+L}$-1, $CHD8_L$-2, or EGFP (control) shRNAs were collected after 24 h and plated in 60-mm culture dishes. Cell number was determined with a hemocytometer after the indicated times. Data are means ± SD of triplicate cultures from a representative experiment.

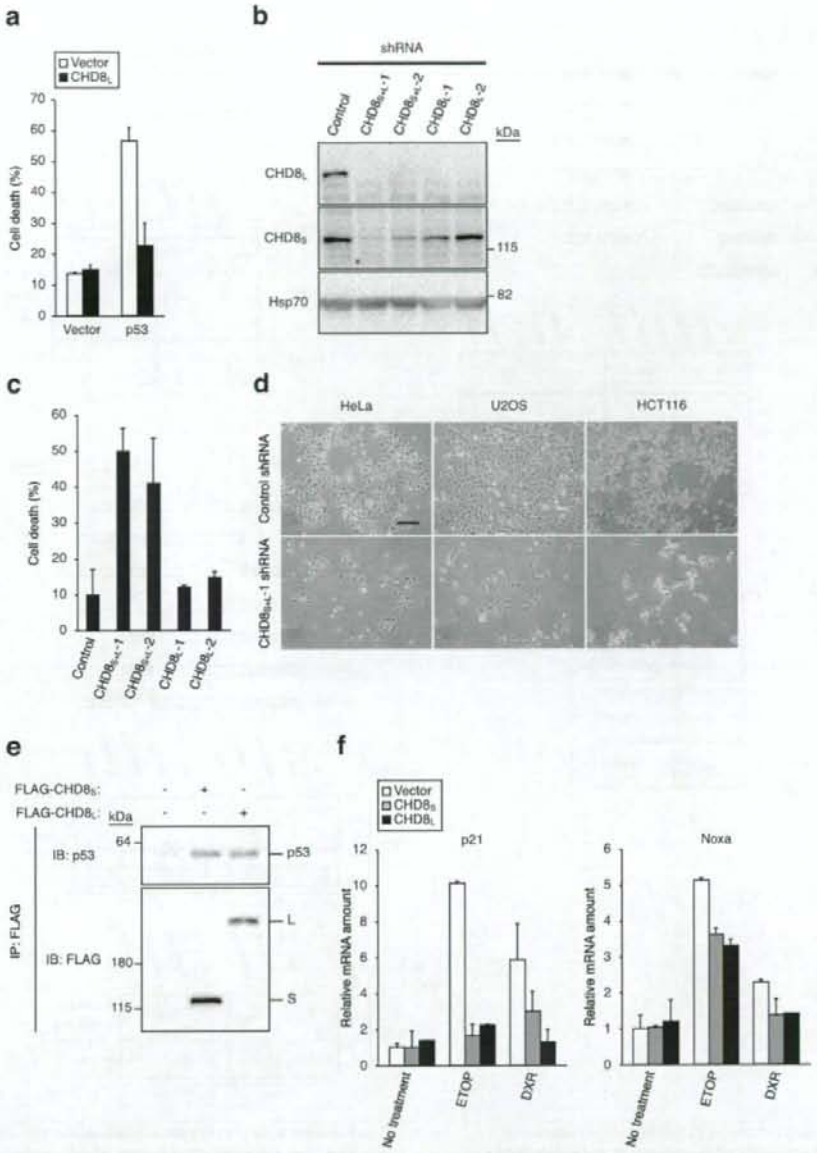

Figure S3 Both $CHD8_S$ and $CHD8_L$ inhibit p53 function. (**a**) U2OS cells were infected with retroviral vectors for $CHD8_L$ or p53 (or with the empty vector) for 72 h. The percentage of dead cells was then determined by trypan blue staining. Data are means ± SD from three independent experiments. (**b**) HeLa cells were infected with retroviral vectors encoding $CHD8_{S+L}$-1, $CHD8_{S+L}$-2, $CHD8_L$-1, $CHD8_L$-2, or EGFP (control) shRNAs. After 96 h, the cells were subjected to immunoblot analysis with anti-CHD8 or anti-Hsp70. (**c**) HeLa cells infected with retroviral vectors encoding CHD8 or EGFP (control) shRNAs were collected after 72 h and stained with trypan blue for determination of the percentage of dead cells. Data are means ± SD from three independent experiments. (**d**) HeLa, U2OS, and HCT116 cells were infected with retroviral vectors for $CHD8_{S+L}$-1 or EGFP (control) shRNAs for 72 h and then examined by phase-contrast microscopy. Scale bar, 100 μm. (**e**) HEK293T cells expressing FLAG-tagged $CHD8_S$ or $CHD8_L$ were incubated with 10 μM MG132 for 8 h and then subjected to immunoprecipitation with anti-FLAG. The resulting precipitates were subjected to immunoblot analysis with anti-p53 or anti-FLAG. (**f**) U2OS cells infected with retroviruses encoding $CHD8_S$ or $CHD8_L$ or with the empty vector were incubated in the absence or presence of etoposide (ETOP) or doxorubicin (DXR) for 24 h and then subjected to quantitative RT-PCR analysis of p21 and Noxa mRNAs. Data are means ± SD from three independent experiments.

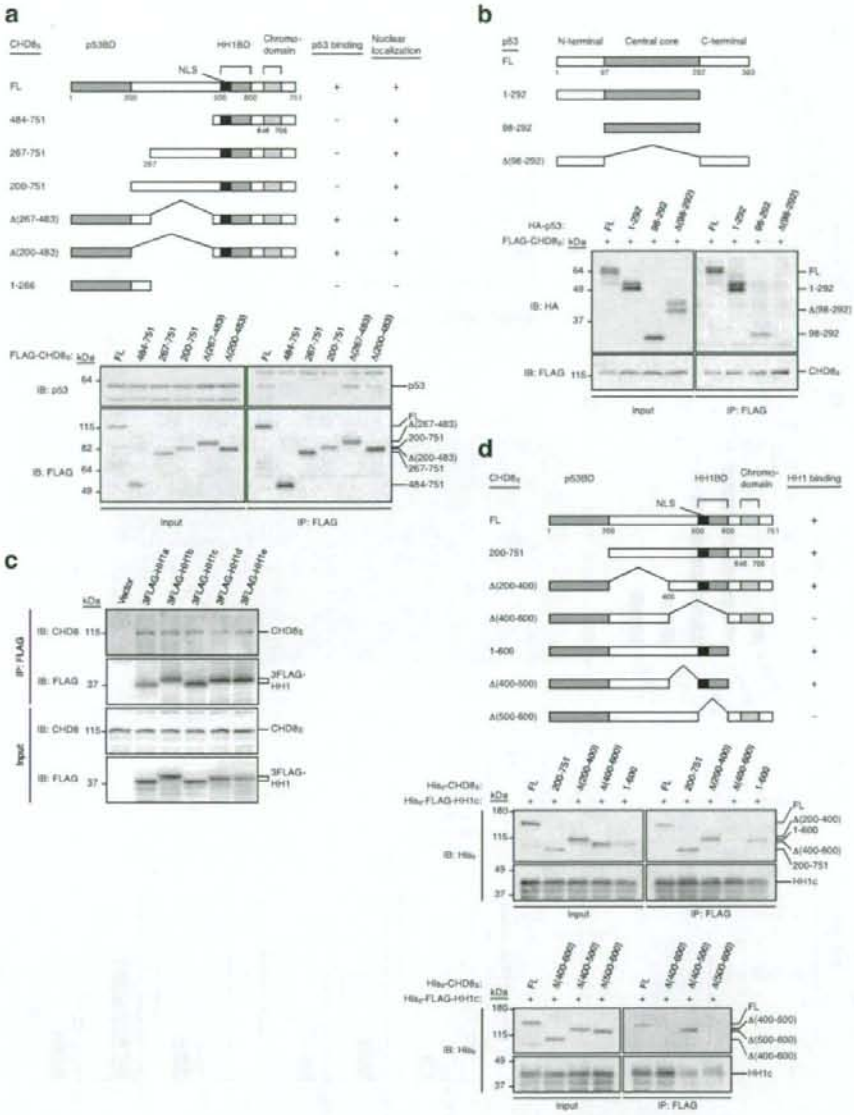

Figure S4 Molecular dissection of p53-CHD8–histone H1 interaction. (**a**) Identification of the region of $CHD8_S$ responsible for binding to p53. HEK293T cells transiently expressing the indicated FLAG-tagged $CHD8_S$ derivatives were subjected to immunoprecipitation with anti-FLAG, and the resulting precipitates (as well as 3% of the input cell lysates) were subjected to immunoblot analysis with anti-p53 or anti-FLAG (lower panel). The results for p53 binding and nuclear localization [determined by immunofluorescence analysis (data not shown)] are summarized together with schematic representations of the $CHD8_S$ derivatives tested (upper panel). p53BD, p53 binding domain; NLS, nuclear localization signal; HH1BD, histone H1 binding domain; FL, full-length. (**b**) Identification of the region of p53 responsible for binding to $CHD8_S$. HEK293T cells expressing the indicated HA-tagged p53 derivatives and FLAG-tagged $CHD8_S$ were subjected to immunoprecipitation with anti-FLAG, and the resulting precipitates (as well as 3% of the input cell lysates) were subjected to immunoblot analysis with anti-HA or anti-FLAG. (**c**) All five major variants of histone H1 interact with CHD8 in vivo. HEK293T cells expressing mouse histones H1a, H1b, H1c, H1d, or H1e tagged with three copies of the FLAG epitope, or those transfected with the empty vector, were lysed and subjected to immunoprecipitation with anti-FLAG. The resulting precipitates, as well as 3% of the original cell lysates (input), were subjected to immunoblot analysis with anti-CHD8 or anti-FLAG. (**d**) Identification of the region of $CHD8_S$ responsible for binding to histone H1. Recombinant His_6-tagged $CHD8_S$ derivatives and His_6- and FLAG-tagged histone H1c (HH1c) were mixed and subjected to immunoprecipitation with anti-FLAG, and the resulting precipitates as well as 10% of the original binding mixtures (input) were subjected to immunoblot analysis with anti-His_6 (right panels). The results of the binding assay are summarized together with schematic representations of the $CHD8_S$ derivatives (left panel).

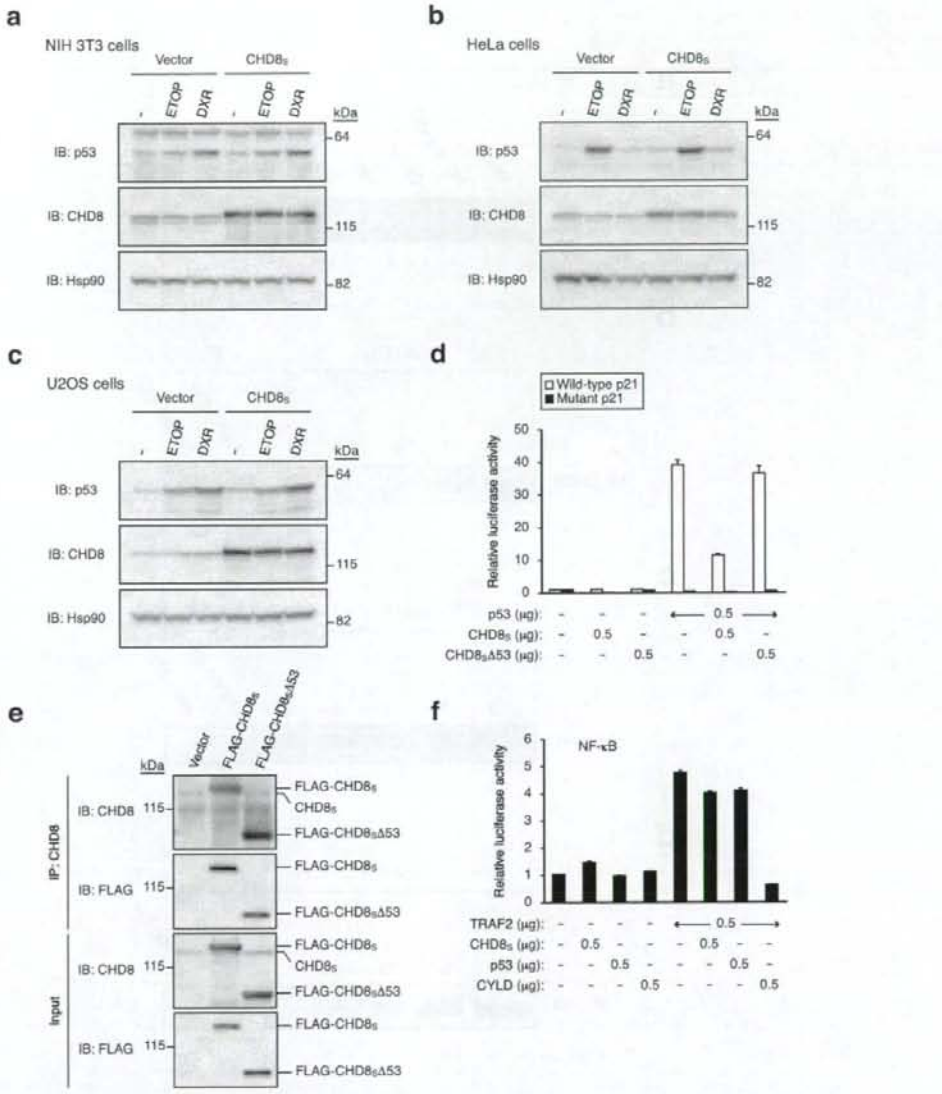

Figure S5 CHD8 is a specific inhibitor of p53-dependent transactivation. (**a**–**c**) Abundance of p53 and CHD8 in cells overexpressing CHD8 and subjected to genotoxic stress. NIH 3T3 (**a**), HeLa (**b**), or U2OS (**c**) cells infected with a retrovirus for $CHD8_S$ or with the empty vector were incubated in the absence (–) or presence of etoposide (ETOP) or doxorubicin (DXR) for 24 h. The cells were then subjected to immunoblot analysis with anti-p53, anti-CHD8, or anti-Hsp90. (**d**) SaOS2 cells were transfected with the indicated amounts of expression vectors for p53 and either wild-type or mutant (Δ53) $CHD8_S$ together with a luciferase reporter plasmid containing wild-type or mutant forms of the *p21* promoter, the latter of which harbored mutations in p53RE1 and p53RE2. The cells were then incubated for 24 h before assay of relative luciferase activity. Data are means ± SD of triplicates from a representative experiment. (**e**) HEK293T cells transiently expressing FLAG-tagged wild-type or mutant (Δ53) $CHD8_S$ were subjected to immunoprecipitation with anti-CHD8. The resulting precipitates, as well as 3% of the original cell lysates (input), were subjected to immunoblot analysis with anti-CHD8 or anti-FLAG. (**f**) HEK293T cells were transfected with the indicated amounts of expression vectors for TRAF2, $CHD8_S$, p53, and CYLD together with a luciferase reporter plasmid containing three binding sites for NF-κB. The cells were then incubated for 24 h before assay of relative luciferase activity. TRAF2 expression increased the luciferase activity derived from this construct, but this effect of TRAF2 was not inhibited by overexpression of $CHD8_S$ or p53. In contrast, CYLD, a deubiquitinating enzyme that is a negative regulator of the NF-κB signaling pathway, markedly inhibited the TRAF2 effect. Data are means ± SD of triplicates from a representative experiment.

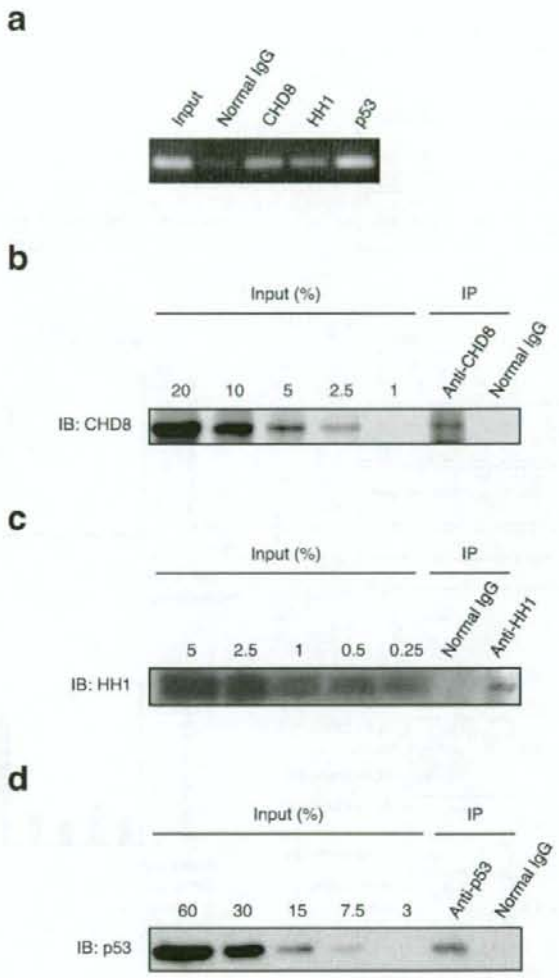

Figure S6 Antibody specificity and immunoprecipitation efficiency for ChIP. (**a**) U2OS cells infected with a retroviral vector encoding $CHD8_S$ were incubated with etoposide for 24 h, lysed, and subjected to ChIP with anti-CHD8, anti-histone H1, or anti-p53 or with control IgG. The precipitated DNA (as well as 1% of the input cell lysates) was subjected to PCR analysis with primers specific for p53RE1 of the *p21* promoter. (**b**–**d**) U2OS cells treated as in (**a**) were subjected to ChIP with anti-CHD8 (**b**), anti–histone H1 (**c**), or anti-p53 (**d**). The resulting precipitates as well as the indicated percentages of the original cell lysates (input) were subjected to immunoblot analysis with the corresponding antibodies. By comparing the amounts of input and immunoprecipitated proteins, we determined the ChIP efficiency to be ~5% for CHD8 (**b**), 0.1% for histone H1 (**c**), and 15% for p53 (**d**).

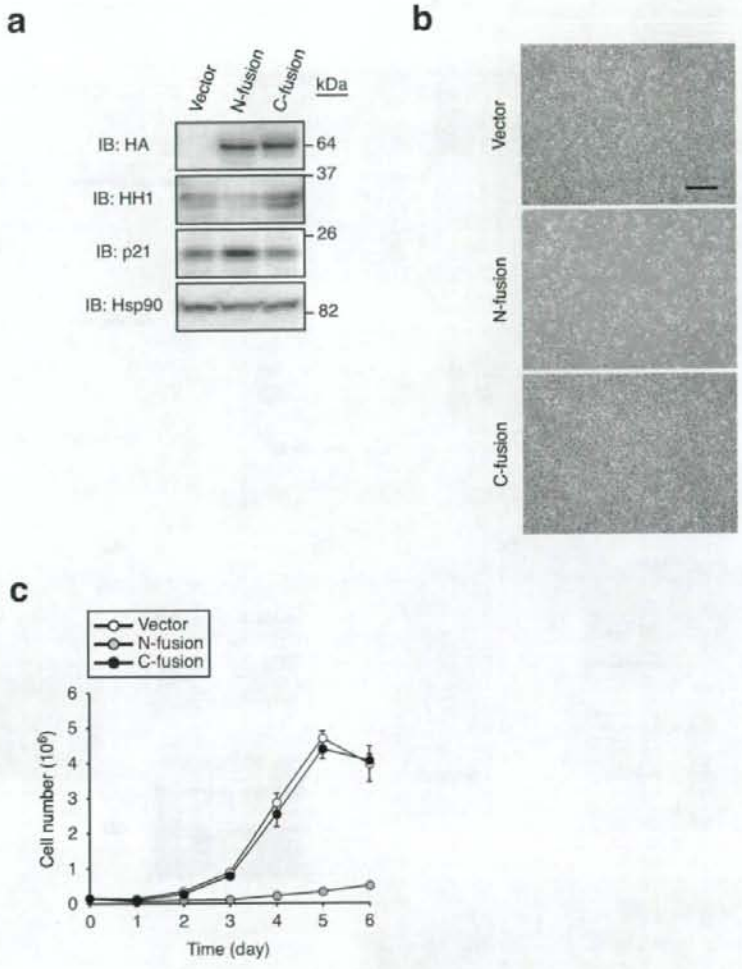

Figure S7 Effects of expression of histone H1 mutants. (**a**) NIH 3T3 cells were infected with retroviral vectors encoding histone H1 tagged at its NH_2-terminus (N-fusion) or COOH-terminus (C-fusion) with EGFP (or with the empty vector) for 96 h and were then subjected to immunoblot analysis with anti-HA (both fusion proteins were also tagged at their NH_2-termini with HA), anti-histone H1, anti-p21, or anti-Hsp90 (loading control). (**b**) NIH 3T3 cells infected as in (**a**) were examined by phase-contrast microscopy. Scale bar, 100 μm. (**c**) NIH 3T3 cells (1.5×10^5) infected as in (**a**) were collected after 24 h and plated in 60-mm culture dishes. Cell number was determined with a hemocytometer after the indicated times. Data are means ± SD of triplicate cultures from a representative experiment.

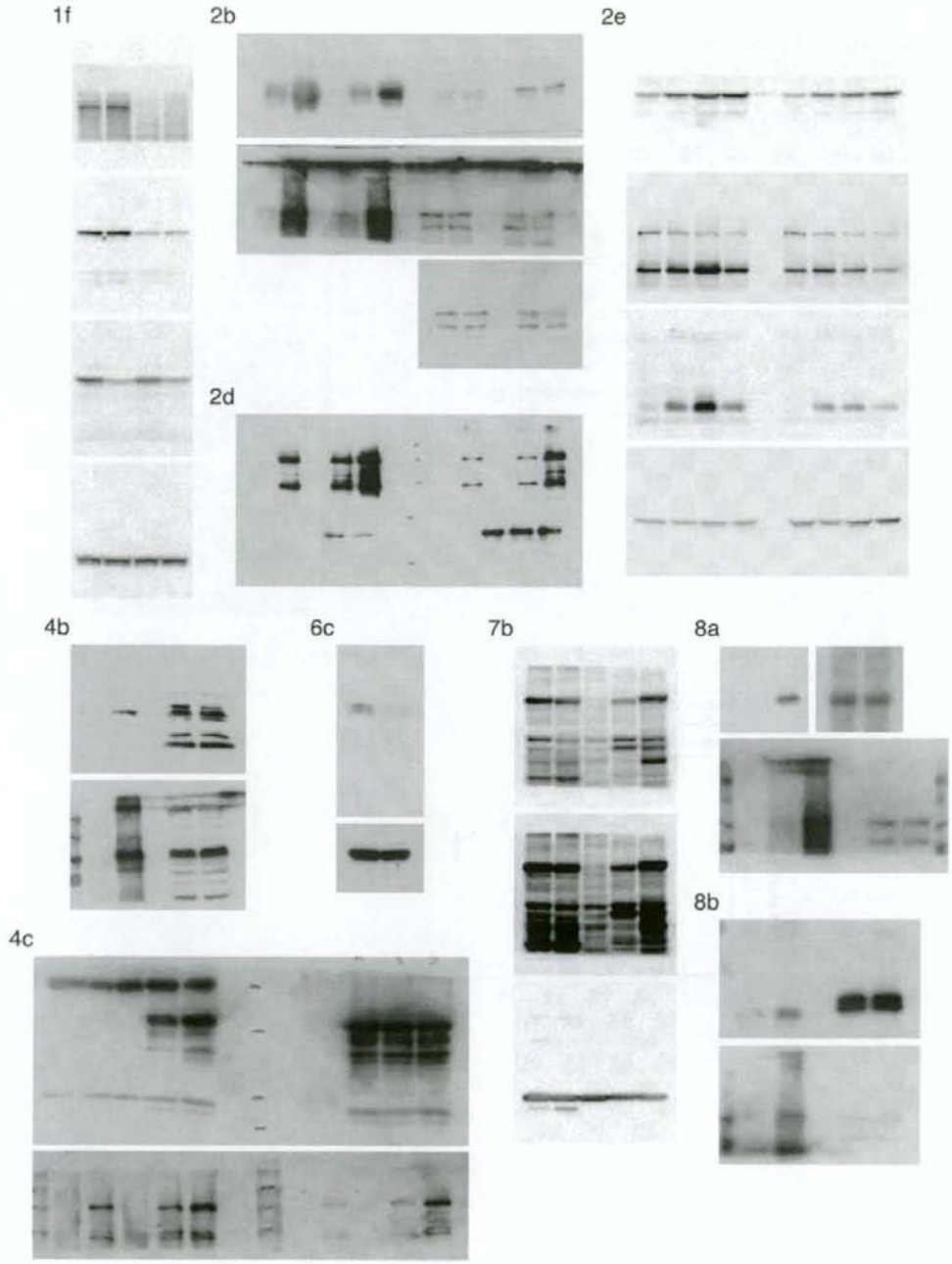

Figure S8 Full scans of key immunoblots in the indicated figures.

Table S1. Identification of CHD8-associated proteins by proteomics analysis.

Gene symbol	Protein name	Sequence coverage (%)
HIST1H1E/HIST1H1C/HIST1H1D	Histone 1; H1e or H1c or H1d	23.5
KPNA2	Karyopherin alpha 2 (RAG cohort 1, importin alpha 1)	22.3
KPNA1	Karyopherin alpha 1 (importin alpha 5)	18.2
KPNA3	Karyopherin alpha 3 (importin alpha 4)	16.6
KPNB1	Karyopherin (importin) beta 1	14.4
KPNA4	Karyopherin alpha 4 (importin alpha 3)	11.7

HEK293T cells transiently expressing FLAG-tagged $CHD8_S$ were subjected to immunoprecipitation with anti-FLAG, and the resulting precipitates were subjected to LC–MS/MS analysis. Proteins reproducibly detected in four independent experiments are listed. The percentage sequence coverage for each protein is also shown.

Table S2. Genotype of embryos from *Chd8*$^{+/-}$*p53*$^{+/-}$ mouse intercrosses.

E7.5	*p53*$^{+/+}$	*p53*$^{+/-}$	*p53*$^{-/-}$	Total
Chd8$^{+/+}$	4	9	3	16
Chd8$^{+/-}$	7	14	5	26
Chd8$^{-/-}$	2	5	3	10
Total	13	28	11	52

E8.5	*p53*$^{+/+}$	*p53*$^{+/-}$	*p53*$^{-/-}$	Total
Chd8$^{+/+}$	2	7	3	12
Chd8$^{+/-}$	9	26	11	46
Chd8$^{-/-}$	1	5	3	9
Total	12	38	17	67

E9.5	*p53*$^{+/+}$	*p53*$^{+/-}$	*p53*$^{-/-}$	Total
Chd8$^{+/+}$	5	16	8	29
Chd8$^{+/-}$	10	36	10	56
Chd8$^{-/-}$	0	4	8	12
Total	15	56	26	97

Embryos from *Chd8*$^{+/-}$*p53*$^{+/-}$ mouse intercrosses were dissected from uteri between E7.5 and E9.5 and genotyped by PCR.

Table S3. Primer sequences (5′→3′) for nested PCR, RT-PCR, and ChIP analyses.

Gene (primer)	Forward primer	Reverse primer
	Nested PCR	
mp53 (Mutant-1st)	GTGTTCCGGCTGTCAGCGCA	AGCGTCTCACGACCTCCGTC
mp53 (Wild type-1st)	ACACACCTGTAGCTCCAGCAC	AGCGTCTCACGACCTCCGTC
mp53 (Mutant-2nd)	CCCGGTTCTTTTTGTCAAGAC	ATGTGCTGTGACTTCTTGTAG
mp53 (Wild type-2nd)	TGGGGAGGCCAAAGTGGGAGG	ATGTGCTGTGACTTCTTGTAG
mChd8 (Mutant-1st)	TGCTAAAGCGCATGCTCCAGACTG	AACTCCGTAACCATTTGTCTATTC
mChd8 (Wild type-1st)	TATAGATTTCCTGTTTGATTTTCC	AACTCCGTAACCATTTGTCTATTC
mChd8 (Mutant-2nd)	ATGCTCCAGACTGCCTTGGGAAAA	GAAACAATGTAAAACAGGCAAATG
mChd8 (Wild type-2nd)	AAAGAATCACACTAGATCTAATCC	GAAACAATGTAAAACAGGCAAATG
	RT-PCR	
$mChd8_S$	CAGATGAGACACTTCTTTCATGAA	TTCTCCGCGCCCAACTCAC
$mChd8_L$	CAGATGAGACACTTCTTTCATGAA	TTTTACCAGGTAGTAAATTACAGG
mp21	TGTCTTGCACTCTGGTGTCTGAGC	TCTTGCAGAAGACCAATCTGCG
hp21	CTGAGACTCTCAGGGTCGAA	CGGCGTTTGGAGTGGTAGAA
mNoxa	ACTCAGGAAGATCGGAGACAAAGTG	ACACTCGTCCTTCAAGTCTGCTGG
hNOXA	AGAGCTGGAAGTCGAGTGT	GCACCTTCACATTCCTCTC
mGapdh	GCCTGGAGAAACCTGCCAAGTATG	GAGTGGGAGTTGCTGTTGAAGTCG
hGAPDH	GCAAATTCCATGGCACCGT	TCGCCCCACTTGATTTTGG
	ChIP	
hp21 (p53RE1)	CAGGCTGTGGCTCTGATTGG	TTCAGAGTAACAGGCTAAGG
hp21 (p53RE2)	GGTCTGCTACTGTGTCCTCC	CATCTGAACAGAAATCCCAC
hp21 (CR)	GGTGCTTCTGGGAGAGGTGAC	TGACCCACTCTGGCAGGCAAG
hBAX (p53RE)	TTGGAAGGCTGAGACGGGGTTATC	AGAAGTTTCGGGCAGGGTTTGAG
hBAX (CR)	CCTGCTGATCTATCAGCACAG	GCTGGTCTCTGAACTCCCAGA
hp27	CCGCCGCCGCAACCAATGGAT	GGAGTCGCAGAGCCGTGAGCA

Mouse and human genes are indicated by m and h, respectively.